Polymer Composites

WILEY | spe INSPIRING PLASTICS PROFESSIONALS

RESEARCH ARTICLE OPEN ACCESS

Developing a Heterogeneous Attenuation Model for Fiber Reinforced Thermoplastic Composites in the Kilohertz Region of the Ultrasonic Spectrum

Austin D. Bedrosian[1] | Andrew Hrymak[2] | Gisela Lanza[3] | Michael R. Thompson[1]

[1]Department of Chemical Engineering, CAPPA-D/MMRI, McMaster University, Hamilton, Ontario, Canada | [2]Department of Chemical and Biochemical Engineering, University of Western Ontario, London, Ontario, Canada | [3]Institute of Production Science (wbk), Karlsruhe Institute of Technology (KIT), Karlsruhe, Germany

Correspondence: Michael R. Thompson (mthomps@mcmaster.ca)

Received: 16 November 2025 | **Revised:** 12 January 2026 | **Accepted:** 2 February 2026

Keywords: active ultrasonics | attenuation | genetic programming | non-destructive testing | polymer composites

ABSTRACT

This study experimentally investigated the discrete phase contributions of fibers and entrapped air on the attenuation spectrum of a fiber-filled thermoplastic composite and derives a mathematical expression for sound attenuation in this heterogeneous material. The frequency-domain attenuation spectrum found with a parts inspection system using ultrasonic guided waves showed two notable spectral fingerprint regions, each corresponding to different material features of the composite. The first region (250–310 kHz) displayed significant sensitivity to the porosity and fiber content in the test specimens, with these two material features found to influence the symmetric S1 dispersion mode phase velocity. An expression describing the attenuation spectrum in this region was developed for the heterogeneous material with the aid of genetic programming algorithms to describe its dependencies on entrapped air and fiber content. Attenuation displayed a linear relationship with frequency in the second region (310–500 kHz), resembling the dampening nature seen with homogenous dispersive materials. A simpler mathematical expression was proposed for this region showing only dependency on whether short glass fibers or carbon fibers were present. The two expressions together capture the ultrasound dampening dominated by material features in the studied thermoplastic composite.

1 | Introduction

Industrial digitization techniques are growing in interest for polymer composite manufacturing. The ability to collect data from connected systems in order to maintain/improve product quality while seeking more sustainable practices has economic and societal benefits [1]. The concept of a smart factory allows one to aim for analysis of a production line in real time, eliminating the normal constraints of having to wait for test results long after a part has been manufactured. One monitoring technology that has shown robust implementation in the smart factory is acoustics, which generally relies upon propagating guided waves at frequencies in the audible range as well as at higher frequencies in the kilohertz to terahertz ranges. For the automotive industry, acoustics have been shown to be a promising technology for evaluating composite materials, having been used in a variety of applications such as fiber orientation predictions, fiber/matrix damage detection, and creep evaluation [2–6]. To effectively analyze these properties using acoustics in a fast-moving manufacturing setting requires the strongest possible signal so that the information stands out from the noise and analysis is made of only the relevant frequency regions for part/material characterization in order to offer real-time feedback.

Sound waves traveling through a material are not 100% efficient, since attenuation is normal in both homogenous and heterogeneous material systems [7]; however, this loss is not uniform in polymers and often varies based on the frequency of the

Highlights

- Attenuation in heterogeneous composite material displays two frequency regimes.
- Dampening was dependent on the fiber type, fiber content, and porosity.
- Genetic programming tool was found useful in developing the attenuation model.

sound wave and the material in question [8]. This loss in signal strength is attenuation (α) due to acoustic dispersion which current models capture by assuming the materials are homogenous regardless of its composition and influenced by frequency (f) using both dampening (d) and scattering (s) terms:

$$\alpha = \alpha_d + \alpha_s = C_d \cdot f + C_s \cdot f^n \quad (1)$$

The dampening term behaves similarly in most dispersion models, even when the microstructure of the material itself is quite different, whereas the power factor for the scattering term will change significantly. For example, large-grained aluminum alloys follow the Mason-McSkimin expression which estimates attenuation by the linear relationship (Equation 1) with quartic frequency dependency for the scattering term [9]. Alternatively, gray cast iron follows a Datta-Kinra expression where Equation (1) has a quadratic frequency dependency for the scattering term [10]. In the case of unidirectional fiber-reinforced polymers, at least one study has found the scattering term to have a cubic frequency dependency [11] though model suitability was questionable in this case due to the distinctive heterogeneity at the meso- and macro-scale with polymer composites compared to these other examples. All expressions found in the literature correspond to offline analysis of solid parts.

The dispersion models found in the literature were all developed for acoustic sensing systems based on signal frequencies in the megahertz region where attenuation is a major concern. In the ultrasonic region (kHz), the magnitude of signal attenuation is much lower, which is a significant benefit for using this region for smart manufacturing systems. This means that lower strength signal can be used which may avoid any microstructural changes or damage induced by the sound emitted into the test material. Another benefit to collecting information in the ultrasonic rather than megahertz region is the signal requires a less costly acquisition and storage system, allowing for faster data processing time for real-time monitoring [6]. For composite applications, the authors have already shown that the ultrasonic region can be used for accurate fiber orientation predictions [6] and fiber length predictions [12].

Unidirectional fiber-reinforced polymer composites experience a cubic frequency dependency for the scattering term of Equation (1), only describing attenuation as a function of frequency while omitting information on its discrete phases corresponding to the fibers present and common processing defects like entrapped air bubbles. Both factors have been shown to influence attenuation in the megahertz region [8, 13, 14]. Scattering models for polymer composites were subsequently developed to relate attenuation with porosity, expanding on the dampening and scattering relation [15–18]. However, these models were all developed at fixed fiber content and do not explore the influence of changing fiber content. This is an important oversight in practice since attenuation in polymer composites has been shown to change significantly as the fiber content increases [14, 19], meaning that large discrepancies are likely present in developed attenuation models (including both fitted and micromechanical models). The ability to capture the heterogeneity of composite materials for their porosity and fiber content within a single attenuation model remains a challenge to be resolved.

The purpose of this study was to quantify the influences of entrapped air, fiber content, and testing frequencies (in the ultrasonic region) on attenuation within polymer composites and devise a descriptive model to improve acoustic monitoring systems for use in smart factories. The intent of the model was two-fold: to provide designers with a means to more accurately predict the sound dampening properties experienced with similar polymer composites (ex. passenger cabin design in vehicles); and to support our own research in frequency domain-based acoustic monitoring methods for quality assurance in the polymer industry. The inclusion of entrapped air in the model was deemed relevant despite being a processing defect due to the difficulties in their complete elimination by practical processing methods. The modeling element of the study was aided with the use of genetic programming, an artificial intelligence tool capable of proposing mathematical terms for the new dispersion model most likely to describe the influences of entrapped air, fiber content, and signal frequency seen in the collected data.

2 | Materials and Methods

2.1 | Materials

The chosen polymer matrix was an extrusion-grade HL781G isotactic polypropylene (LyondellBasell; Texas, USA) supplied in pellet form. Two common industrial rigid fibers were chosen for reinforcement, with sizing specified for polypropylene applications: Owens Corning E-glass fiber with an average fiber length and diameter of 4 mm and 14 μm, and Zoltek carbon fiber with an average fiber length and diameter of 4 mm and 12 μm, respectively. The fibers were dried at 80°C for 24 h prior to use to minimize moisture. Polybond 3200 maleated polypropylene compatibilizer (SI Group; New York, USA) was used to improve cohesion between the polypropylene and the respective fibers.

2.2 | Composite Preparation

A Thermo HAAKE Rheomix 3000 batch mixer (Thermo Fisher Scientific; Massachusetts, USA) was used to compound the different composite formulations used in the study. The batch mixer was operated at 230°C and a rotor speed of 60 RPM. Three fiber loadings of 5, 15, and 25 vol% were chosen for both the glass fiber and carbon fiber composite samples. The necessary amount of polypropylene and 1.5% (w/w) maleated polypropylene were fed into the batch mixer simultaneously and mixed until the torque leveled off. The fibers were gradually fed into the batch mixer at this point to limit clustering of the fibers within the polymer melt. The composite melt (200 g) was mixed until the torque

leveled off, allowing for the fibers to be properly incorporated with the melt.

The composite melt was immediately transferred to a 90 mm x 90 mm x 2.5 mm mold sandwiched between two metal plates and then placed within a hot press (Model 4389 Carver hydraulic press; Indiana, USA). The hot press was preheated to 230°C to prevent the melt from cooling prior to molding. The platens were pressed with a two metric tons load for 2 min and then six metric tons load for an additional 2 min before being water-cooled while still at six metric tons load until the mold reached 80°C. Solidified plaques rested at room temperature for 1 week prior to testing. An example of a plaque can be seen in Figure 1. The yellowing and spottiness of the sample were done intentionally for thermographic imaging testing; however, their results were not included in this thesis.

2.3 | Micro Computed Tomography

A Zeiss Metrotom micro-computed tomography device (ZEISS; Oberkochen, Germany) located at the Karlsruhe Institute of Technology (Karlsruhe, Germany) was used to analyze the composite plaques and identify the location and quantity of entrapped air within. The plaques were placed within an ultralight foam mount and placed into the μCT machine, which can be seen in Figure 1. The voltage, current and gain of the x-ray tube were varied to optimize the voxel resolution; a voltage of 130 kV, current of 90 μA and gain of 2.5 times were used resulting in the voxel resolution of the μCT to be 29.92 μm with a focal spot size of 20 μm. The μCT machine mode was set to fast, allowing the plaques to be continuously scanned in a single 360° rotation without the machine pausing for each projection. This drastically decreased the time to complete each plaque characterization. No X-ray filters were used during the μCT scans. Multiple scans of the plaques were done, varying the position within the ultralight foam mold where X-rays would be primarily targeting. The plaques would be positioned to target the middle center of a plaque, the upper left region of a plaque the upper right region of a plaque and lower center region of a plaque. The plaques were reconstructed from the μCT projections using VGStudioMax. The built-in porosity analysis tools were used to determine the location and quantity of entrapped air within each plaque. Using the software, pores with a diameter greater than 0.07 mm could be identified, creating a distribution of entrapped air. The variation of overall entrapped air within the plaques based on scanning position were found to be less than 0.2 vol% for the glass fiber plaques and 0.17 vol% for the carbon fiber plaques.

2.4 | Acoustic Setup

The offline active ultrasonic method was adapted from previous work for composite fiber orientation analysis [6]. Emitter (resonant type, R15 α) and receiver (broadband type, F30 α) ultrasonic sensors (Physical Acoustic Corporation; New Jersey, USA) were placed on either side of a composite plaque and tested. The emitter and receiver were placed on either side of the plaque for through-plane transmission at the same targeted positions where the porosity was previously characterized by μCT scans, being affixed to the composite surfaces with a silicone vacuum grease (Dow Corning; Michigan, USA). Since the plaques were opaque, a custom 3-D printed rig was used to ensure the sensors aligned over one another. For this study there was no need to offset the sensors. This rig eliminated any centroid offset between the emitting and receiving sensor, even if a plaque may contain a slight curvature; once the sensors were correctly aligned the rig was removed. A 10 MHz WaveForm generator paired with custom Command Expert script (Keysight; California, USA) was used to analyze 250 consecutive square waveforms. The frequencies chosen were from 250 to 500 kHz, with a maximum amplitude at 5 V detected signal. This region was chosen as dispersion mode and fiber resonance exist within this range of frequencies for fiber-filled composite materials [6, 20]. The frequencies below 250 kHz were omitted due to them being outside of the sensitive frequency range for the sensors [21]. The received signal for each waveform was recorded with a 12-bit 4-channel 10 MHz data acquisition system (National Instruments; Texas,

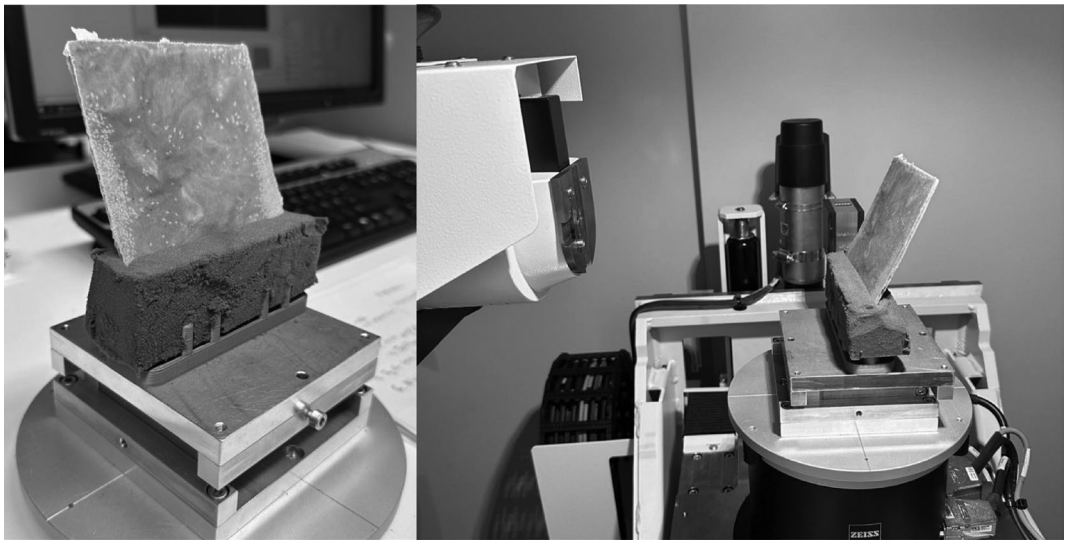

FIGURE 1 | Micro-computed tomography testing of a glass-fiber reinforced polypropylene plaque. (Left image) is the mount used to hold the plaque, where the plaque is placed in an ultralight foam. (Right image) is the mount fastened within the tomography machine.

USA), with a sampling rate of 3 MHz and a noise threshold of 0.06 V to limit noise. No signal amplification was done for this study.

The attenuation coefficient (α) was calculated using the Beer–Lambert law at each frequency, comparing the ratio of the maximum amplitude of the recorded waveform after transmission through the composite plaque with the maximum amplitude emitted waveform prior to transmission (5 V). This can be expressed by calculating α (Neper per mm) using Equation (2), where I is the recorded maximum amplitude (volts), I_0 is the initial maximum amplitude of 5 V and x is the caliper-measured plaque thickness (mm).

$$\alpha = -\frac{1}{x} \cdot \mathrm{Ln}\left(\frac{I}{I_0}\right) \tag{2}$$

The attenuation coefficients for each frequency were then combined to create an attenuation spectrum. Processing was done using code developed in Python (version 3.11) with the NumPy library (accessed November 8th, 2023) [22].

2.5 | Dispersive Mode Calculation

Dispersive modes were calculated by a modal analysis to confirm their presence within the Symmetric Region, a distinctive range of frequencies in the collected acoustic spectra that is discussed in detail in the Results and Discussion section. The calculations were done using the open-source *Lamb-Wave-Dispersion* Python package (Version 0.0.0) [23]. The rule of mixtures was used along with reported data for polypropylene and the glass and carbon fibers in order to calculate the dispersion modes; the dispersion curves were calculated assuming the composites were entirely solid and uniform in properties [24–27]. The calculations were done for both fibers at the varying volume percentages to provide an understanding of how the Symmetric Region attenuation response deviated from the theoretical frequencies [20] when air was introduced. It should be stated that these calculations provide a theoretical basis to which the experimentally tested attenuation spectra can be compared. As these calculations are used for homogenous materials, they will not incorporate the effects of scattering from the fibers or entrapped air, making them excellent for making comparisons between how a perfectly homogenous material would act versus a heterogeneous material with enclosed defects.

2.6 | Genetic Programming

The artificial intelligence tool 'Genetic Programming' aided in developing a mathematical expression for attenuation that incorporated fiber content, entrapped air volume and frequency of the acoustic signal in its determination; the model was trained with glass fiber composite data and then tested on results for either glass- or carbon-fibers to evaluate whether the expression was fiber type specific. Each variable of study was mean-centered and standardized using their mean and standard deviation. The means for the four variables were 0.514 Np/mm, 280 kHz, 1.500% and 14.850%. The standard deviations were 0.150 Np/mm, 17.607 kHz, 0.694% and 8.067%. A custom script using the *GPlearn* Python library for genetic programming (GP), paired with a NVIDIA GeForce GTX 1650 Super GPU, was created using terms found in historical attenuation models (discussed in the Introduction); the chosen terms were addition, subtraction, multiplication, division, square roots, inversion and the use of negative numbers; additional terms were initially considered based on logarithmic and trigonometric functions but the resulting expression was overly complex due to over-fitting of the data. Constants were constrained between −100 and 100 so that they remained at a similar magnitude to the mean-centered and standardized data. For GP model development, the glass fiber data was randomly split into training and testing sets on a 2:1 ratio, with both sets containing results for each fiber content. Symbolic regression was chosen for genetic programming to develop the equation relating the three characteristic variables (frequency, porosity and fiber content) to the response variable, attenuation.

A tuning process to create the best fitting attenuation mathematical expression to the experimental data was done by varying the probabilities of the parent genes being passed down to the child in the GP model. The probabilities used throughout this study were probability of gene crossover between tournament winners; probability of crossover genes mutating; probability genes would be removed (to help eliminate poor performing genes and limit bloating); probability a gene would randomly mutate (not during crossover); and probability a gene would be replaced by an existing gene. The various genetic programming probability ranges used were tabulated in Table 1, with the probabilities of all genetic permutation outcomes equaling 100%. To minimize the size of an expression, the parsimony coefficient (a penalty metric to combat bloat) was varied from 0.01 to 0.001. Additionally, the maximum number of generations was constrained, with four hard constraints of 5, 10, 50 and 100 generations chosen. While the above probabilities were varied, the following hyperparameters were kept consistent for all genetic probabilities: population size was 5000; the fitness was the mean square error with a termination stopping criteria of 0.001.

Model form determination was done in Python using the SciPy library. The mean square error between experimental attenuation and calculated attenuation from the optimized terms was the chosen objective function. Various solver methods were tested to determine which would give the optimal results: Nelder–Mead, Limited memory BFGS, Truncated Newton Constrained, Constrained Optimization by Linear Approximation, and Sequential Least Squares Programming methods. Each solver

TABLE 1 | Genetic programming probability ranges used throughout the study.

Probability parameter	Range (%)
Gene crossover between tournament winners	[60, 90]
Gene crossover mutation	[1, 10]
Gene removed	[1, 15]
Gene mutation (not during crossover)	[1, 10]
Gene replacement	[1, 5]

repeatedly ran 10 times independently with the starting point changed for each iteration using the NumPy *random.default_rng()* function to ensure the solution was not a local minima. The stopping criteria for each run was 0.001, or a maximum iteration of 10,000. The results for the optimized expressions are discussed in Section 3.

3 | Results and Discussion

3.1 | Nature of Material Attenuation Based on Spectral Regions

The characteristic attenuation coefficients for both glass- and carbon-fiber filled polypropylene composites over the tested frequency range (250–500 kHz) exhibited two distinctly different acoustic behaviors, as shown in Figure 2; the frequency range was chosen to cover the known beam harmonic resonance of these types of fibers in the polymer matrix [12, 28]. The region between 250 and 310 kHz included a minimum centered near 280 kHz, which is atypical of homogenous dispersive materials, whereas the region between 310 and 500 kHz was expected of polymers and showed linearly increasing attenuation with frequency. These two regions are analyzed separately in this study, though both regions appear to be significant in describing both glass- and carbon-fiber filled thermoplastic composites.

3.1.1 | Symmetric Region [250–310 kHz]

The attenuation in this range displayed a unique profile. There is a symmetrical nature to the attenuation profile in this range of frequencies around a minimum centered at ~280 kHz, which was found with both glass and carbon fiber-filled composites, as shown in Figure S1 (supplementary documentation). For clarity, the frequency corresponding to the lowest attenuation coefficient value in these minima will be referred to as the vertex frequency in this study. The vertex frequency and amplitude of the minima were examined to establish their dependency on the main test variables, namely the composite fiber volume content v_f and porosity ϕ (entrapped air content).

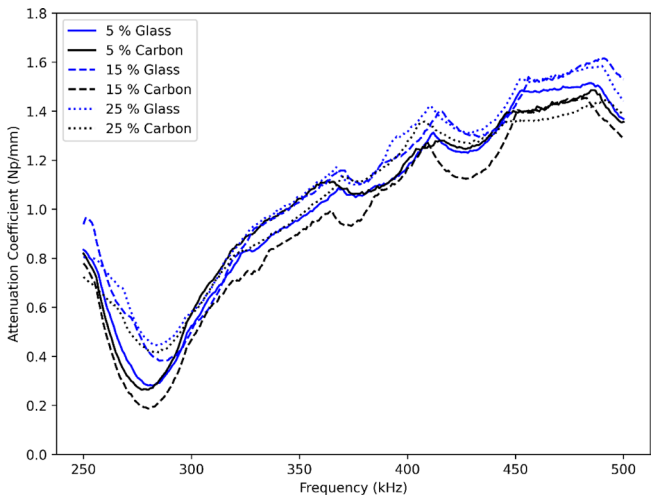

FIGURE 2 | Average calculated attenuation coefficients (Np/mm) for both glass fiber (blue) and carbon fiber (black) reinforced polypropylene composites with a testing range of 250–500 kHz. The frequency resolution is every 1 kHz. The solid lines (–) represent the 5 vol% results, the dashed lines (– – –) represent the 15 vol% results and the dotted lines (. . .) represent the 25 vol% data.

With regards to fiber content, increasing glass fiber content was found to statistically increase the vertex frequency (p-value of 0.01); however, there was no influence for carbon fibers (p-value of 0.826). In general, the influence of fiber content was minor compared to the effect of porosity on the vertex frequency, as will be shown below. Conversely, the amplitude of the vertex frequency increased with increasing fiber content for both glass fibers (p-value of 0.004) and carbon fibers (p-value of 0.035).

With regards to the porosity measured by μCT, the vertex frequency was found to increase with increasing porosity even at the low porosity present in the fiber-filled composites ($\phi = 0.48\%–2.23\%$). As shown in Table 2; the influence of porosity was statistically significant with glass fibers (p-value of 1.38×10^{-5}) but not for carbon fibers (p-value of 0.127). A deeper investigation regarding this is discussed in Section 3.2. Being the most influential variable in the study on attenuation, Figure 3 presents the data and fitted regression expressions for porosity, separately for the glass fiber- and carbon fiber-composite samples.

Interestingly, the fitted models showed nearly identical intercepts, being at 280.38 kHz and 279.23 kHz respectively for the two materials. The amplitude of the attenuation minima was only found to statistically increase with glass fibers (p-value of 0.004) and once again, not for carbon fibers (p-value of 0.122). Because of the seemingly low sensitivity of attenuation to fiber content and porosity for carbon fiber composites, the GP modeling was focused on the glass fiber-based results to ensure the influences of these variables were represented correctly. A discussion regarding sensitivity based on fiber type is discussed in Section 3.2.

The behavior of the attenuation minima in this region was considered unique as it showed sensitivity to both fiber content and porosity, in addition to frequency. Normal attenuation behavior for homogeneous dispersive materials is nearly exclusively related to frequency. For heterogenous materials like polymer composites, the inclusion of discrete phases like

TABLE 2 | Porosity ranges determined by μCT scans for the different fiber-filled composites.

Fiber type	Fiber volume fraction	Average porosity (%)	Standard deviation
Glass fiber	5	0.48	0.12
Glass fiber	15	2.27	0.17
Glass fiber	25	2.23	0.45
Carbon fiber	5	0.99	0.08
Carbon fiber	15	1.33	0.05
Carbon fiber	25	1.70	0.37

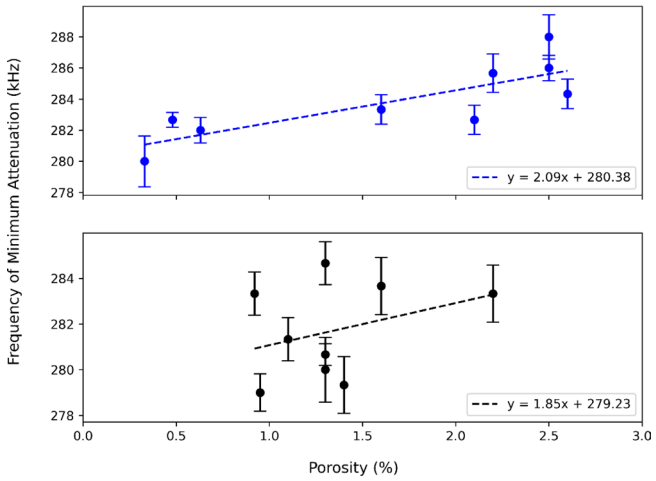

FIGURE 3 | Comparison of the vertex frequency (kHz) with the composite plaque porosity (volume %) for fiber both (Top plot) glass fiber and (Bottom plot) carbon fiber reinforced polypropylene composites. The error bars are the standard deviation at the given porosity. The dashed lines (– – –) are the regressed lines for the vertex frequency on the porosity for both the glass fiber (R^2 of 0.73, p-value of 1.38×10^{-5}) and carbon fiber (R^2 of 0.30, p-value of 0.127).

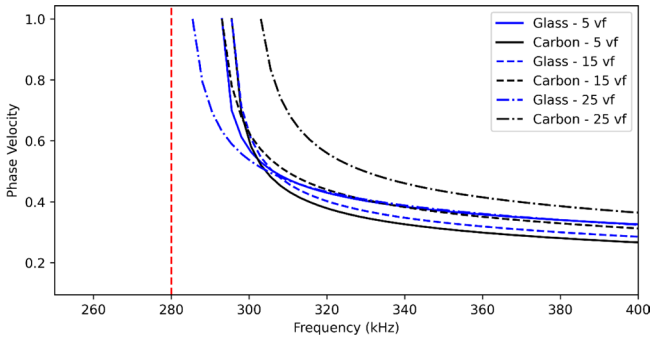

FIGURE 4 | Simulated dispersion symmetric S1 mode results for both glass fiber (blue) and carbon fiber (black) reinforced polypropylene composites. The solid lines (–) represent the 5 vol% results, the dashed lines (– – –) represent the 15 vol% results and the dotted lines (. . .) represent the 25 vol% data. The vertical red line lies at 280 kHz, the y-intercept value for both regressed lines determined in the figure. The *Y*-axis has been normalized to show comparisons between the various conditions.

fibers (and the associated porosity with their addition in melt mixing processes) presents a greater likelihood of material factors influencing sound propagation, thus producing these minima that shifted to increased frequencies and rose in attenuation amplitude with fiber content. Seeking to postulate a unifying explanation for the dependencies seen for both fiber content and porosity on attenuation in this region, two acoustic phenomena were considered: dispersion modes and fiber resonance. The reason for combining theories is that neither fully explains these results. Dispersion affects the velocity of a propagating sound wave based on material and dimensional effects [29], which in the case of this study would be primarily the composite's modulus and density [20]. Calculations showed the Symmetric Region contained an S1 dispersion mode and the fiber's strong resonance frequencies; the S1 dispersion mode corresponding to each fiber content tested in this study is presented in Figure 4. Neither type of fiber, glass versus carbon, showed a significant influence (p-values of 0.522 and 0.454, respectively for glass and carbon) on the phase velocity though higher porosity was shown by others to significantly decrease the speeds of sound [13].

Additionally, the dispersion mode cannot explain why fiber content or porosity are influencing the amplitude of the minima, which is why we believe fiber resonance must be contributing to the attenuation behavior in this region. Heterogeneity material can have a unique effect on attenuation due to acoustic resonance of their discrete phases, feasibly affecting the minima in our case in both amplitude and frequency; glass fiber resonance has already been identified within this frequency region in a previous work [6]. In general, increasing fiber content will amplify the effect of its resonance frequency [30], increasing the signal strength at the associated resonance frequency. With an increased signal strength at the resonance frequency, the vertex frequency would change in a nonlinear manner to reach the resonance frequency. Noting the porosity in this study was associated with fiber content (increasing in value with fiber content), the increased resonance effects with more fibers may also be why the vertex frequency increased with porosity instead of decreased. Unlike dispersion modes, increasing the number of fiber resonance events (by increasing the amount of fibers resonating) increases the material resonance strength and causes the attenuation signal to be reduced at the associated frequency values. The amplitude of the minima may also be explained by the theory of fiber resonance since increasing fiber content will increase the amount of signal scattering within a heterogeneous material and thus increase attenuation. The amount of scattering should similarly increase with porosity. This analysis on the experimental results strongly indicated to the authors that fiber resonance was having a greater impact on the frequency value of the minima compared to dispersion modes and that associated scattering effects generated by the increased inclusions within the material further attenuated the signals.

A mathematical expression for attenuation within this region was derived using the genetic programming (GP) AI tool to explain the influences of porosity and fiber content; original attempts to capture both regions simultaneously were unsuccessful in fitting the data, resulting in the separate analyses. Training of the GP model with the glass-fiber composite acoustic data was purposely done on account of the vertex frequency showing a stronger dependency on porosity with this material whereas inclusion of the carbon data tended to dampen the sensitivity of the predicted expression to this variable; however, testing was done with data of both composites to find the overall best candidate expression and limit overfitting to the glass-fiber results. A total of 32 different permutations of hyperparameters were chosen for the GPlearn algorithm, leading to 32 different equations. The two highest performing equations based on their R^2 that included both ϕ and v_f, are given in Equation (3) and Equation (4). The R^2_{Glass} for the two equations were 0.834 and 0.735, respectively while R^2_{Carbon} were 0.533 and 0.592, respectively. It is worth reminding that α, f, ϕ and v_f are the mean-centered and standardized variables of frequency, porosity and fiber volume fraction, not

the nominal values, hence why they are bolded. These variables are therefore without units.

$$\boldsymbol{\alpha} = \mathbf{f}^2 - \sqrt[4]{|\,\mathbf{f}^2 - 1\,|} + \frac{\boldsymbol{\phi}\left(\mathbf{v_f} - 2 \cdot \mathbf{f}\right)}{19.849} + \frac{\mathbf{v_f} - \mathbf{f}}{8.277 - \mathbf{f}} \tag{3}$$

$$\boldsymbol{\alpha} = \mathbf{f}^2 + \frac{\boldsymbol{\phi}}{18.261 - \boldsymbol{\phi}} - \sqrt{\left|\frac{\sqrt{|\boldsymbol{\phi}|}}{\boldsymbol{\phi} + \mathbf{v_f}}\right|} \tag{4}$$

Both expressions show similarities to Equation (1) for homogeneous materials but are understandably more complex for our heterogenous material by considering the discrete phases of fibers and bubbles on attenuation. Genetic programming was able to identify the strong symmetric relation between signal frequency and attenuation experienced by the composites, though the quality of fit was poorer with carbon fibers rather than glass fibers, as expected based on the modal analysis and resonance behavior discussed above.

The response of fiber content and porosity on the captured equations terms is interesting. For starters, both the third and fourth terms in Equation (3) display clear linear dependencies between attenuation and the fiber content, coinciding with the increasing scattering effects that were observed for both the glass and carbon fibers in the attenuation spectrum. The third term of Equation (3) also demonstrates a linear dependency in the region between attenuation and porosity. As this equation was developed on the glass-fiber results, it makes sense why the effects were captured even if they were not present for the carbon results. When analyzing Equation (4), the behavior becomes more challenging to visualize due to the third term since the attenuation response for both fiber content and porosity becomes dependent on one another. The denominator of the third term will result in division by zero for cases when either factor is zero, or the additive inverse. Increasing either factor also changes the magnitude of attenuation for the entire region in an oscillatory manner. Another issue is that the second term does capture the increasing magnitude of attenuation with porosity. The rational term in the respective domain will always increase attenuation as the porosity increases. The slightly better fit to the data with Equation (4) for the carbon-fiber filled samples can be attributed to the fact the equation itself did not capture any changes to the vertex frequency. Visualizing only the frequency variable of Equation (4), no additional linear terms exist which would shift the vertex frequency.

Considering the limited amount of data (approximately 54 acoustic tests) available for training the GP model, the fit to results and similarity in the form of these two expressions to those in the literature for homogenous materials was considered a positive outcome. The GP method benefits from larger dataset than the 54 tests to predict expressions fully descriptive of the modeled phenomenon but we believe by seeking expressions that were comparable to those for homogenous materials, the risk of overfitting were diminished; similarly, we believe the strategy of separating the data into training and testing sets will reduce fitting errors, allowing the resulting equations to adequately reflect the analyzed region of the spectrum. Both expressions capture the minima of the region; however, the third and fourth terms of Equation (3) better captured its dependency on fiber content as well as porosity across the region than Equation (4). The second term of Equation (4) was unable to mimic the behavior observed for the Symmetric Region relating to changing porosity and resonance effects, and its third term presented challenges with specific fiber content and porosity pairing, resulting in an expression not truly capturing the nature of attenuation for the composite materials.

Ultimately the ultrasonic attenuation in this region of symmetry, which was shown to be influenced by the amount of air and fibers within the composite material, was captured with the help of GPlearn. The ability to capture this region and highlight the effects of both entrapped air and fiber content on attenuation can help identify optimal testing frequencies for quality assurance monitoring.

3.1.2 | Dispersion Region [310–500 kHz]

The Dispersion Region does not display any clear dependencies based on either porosity or fiber content, making its modeling seemingly more straightforward. While there was similarity in attenuation for both fiber types and all tested fiber content at most frequencies in Figure 2, however, between 430 to 500 kHz there appeared to be some distinctiveness based on the fiber type (glass versus carbon). Differences in the attenuation spectra did not increase with fiber content nor porosity. Overall, this region resembled the nature of homogenous dispersive materials where the attenuation increases linearly with frequency.

With genetic programming, porosity and fiber content were still considered as variables in the mathematical terms using the same hyperparameters as used for the Symmetry Region. For the majority of the candidate expressions generated by GPlearn, attenuation was solely dependent on the test frequency. Some expressions added components with the testing frequencies with varying fitting coefficients. These expressions were combined resulting in a combined candidate generated by GPlearn for this region shown in Equation (5):

$$\boldsymbol{\alpha} = \mathbf{f} + \frac{\mathrm{A}}{\mathrm{B} - \mathbf{f}} + \frac{\mathbf{v_f}}{\mathrm{C}} + \frac{\boldsymbol{\phi}}{\mathrm{D}} + \frac{\mathbf{v_f} \cdot \boldsymbol{\phi}}{\mathrm{E}} + \frac{\mathbf{v_f} \cdot \mathbf{f}}{\mathrm{F}} + \frac{\boldsymbol{\phi} \cdot \mathbf{f}}{\mathrm{G}} + \frac{\mathbf{v_f} \cdot \boldsymbol{\phi} \cdot \mathbf{f}}{\mathrm{H}} \tag{5}$$

where A through H are fitting coefficients without units. Working with this expression provided an opportunity to confirm there was significant dependency on fiber content and porosity, which we did by determining the eight coefficients optimally fitted based on three sets of data: combined glass fiber and carbon fiber; glass fiber only; and carbon fiber only. The optimization results for these three datasets are shown in Table 3, indicating that only the first two terms of Equation (5) were influential on attenuation and confirming that fiber content and porosity had no significant effect on sound propagation in this spectral region; this outcome was the same whether all frequencies between 310 and 500 kHz were considered in the training of the GP model or when the highly variable region between 360 and 430 kHz was ignored. At least this outcome validated the

suitability of using genetic programming for this exercise since it showed it was possible to obtain similar expressions as those historical models by this emerging AI technique.

3.2 | Influence of Fiber Type

The diminished sensitivity of the attenuation spectrum to fiber content and porosity for the carbon-fiber composites complicated attempts to create new mathematical expressions. While the proposed expressions for attenuation apply sufficiently well to both glass and carbon fiber composite materials, deeper analysis was required to understand the cause(s) for this difference in sensitivity.

To rationalize the Symmetric Region's sensitivity to fiber type where porosity influences dominated, a closer examination of the μCT scans was felt to be warranted. Examples of defect diameter distributions for the entrapped bubbles by μCT characterizations of both glass fiber- and carbon fiber-filled specimens are provided in Figure S2. The sizes of entrapped air bubbles were larger for specimens containing glass fibers, in the range of 100–800 μm compared to 100–400 μm for those with carbon fibers. The bubble distributions for both fiber types were disproportionately skewed to sizes at the lower end of these ranges. A Kolmogorov–Smirnov (KS) similarity test compared the two size distributions $\left(H_o: Glass(x) \leq Carbon(x)\right)$ and concluded the null hypothesis was rejected (p-value of 2.95×10^{-2}), meaning the bubbles in the glass fiber-filled plaques were larger. Based on this analysis, it is proposed that the influence of porosity on attenuation around the vertex frequency was dependent on the entrapped air being above a critical bubble size (a value between 400 and 800 μm is expected though these is insufficient data to state a specific critical value). To reinforce this finding, μCT scans of the neat polypropylene were also analyzed, showing bubble sizes very similar to those found in carbon fiber-filled plaques, between 100 and 300 μm and just like the carbon fibers-filled plaques, no correlation was found between the vertex frequency and its porosity (p-value of 0.815).

The attenuation spectra in the Dispersion Region showed clearer differences to one another based on fiber type despite porosity having no influence as it did in the Symmetric Region. While the glass fiber-filled spectra showed a high level of parity among themselves, the carbon fiber-filled attenuation spectra showed much more variability in this region. This can be seen in Figure S3. A classification approach was introduced to determine if the attenuation spectra of the Dispersion Region could successfully be classified as either a glass fiber- or carbon fiber-filled sample.

The first test was to determine if the total 54 fiber acoustic signals could be classified based on fiber type. Using the optimized coefficients of Equation (5) for glass only results and carbon only results found in Table 3, all related attenuation spectra for the Dispersion Region were compared using machine learning classifiers; the classifiers of Fisher's Linear Discriminant (FLD) and Support Vector Machines (SVM) used the classification F1 score [31] as their performance metric and considered the only independent variable being frequency. Also for SVM, linear, polynomial and radial basis function kernels were explored. The confusion matrices for the five classifiers can be seen in Figure 5, where both FLD and SVM with either a linear or polynomial kernel were found to be correctly classifying the entire dataset into either a glass sample (class 0) or a carbon sample

TABLE 3 | Optimization results for the eight coefficients of Equation (5) based on which dataset was included during the optimization.

	Optimized coefficient								MSE
Dataset	**A**	**B**	**C**	**D**	**E**	**F**	**G**	**H**	
Glass and carbon	−0.084	1.800	19.067	79.170	11.499	100	97.869	48.585	0.097
Glass	−0.085	1.802	−100	12.731	9.801	99.998	33.990	−31.239	0.064
Carbon	−0.181	1.887	2.962	−2.840	4.729	100	100	−100	0.097

Note: The mean square error is listed in the final column.

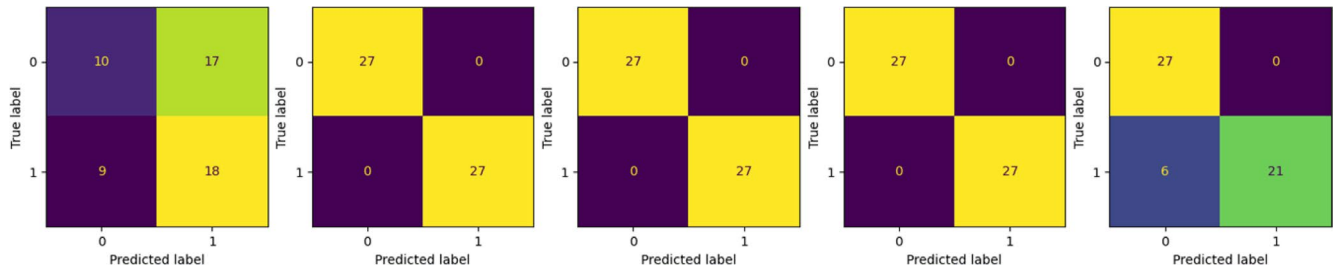

FIGURE 5 | Confusion matrix results for the five classification algorithms used when trained on the entire data set. From left to right the confusion matrices are for the optimization results, Fisher's linear discriminant, support vector machine with a linear kernel, support vector machine with a polynomial kernel and a support vector machine with a radial basis function kernel. The amount of glass fiber results (Class 0) that were correctly classified will be listed in the top left quadrant; the amount of glass fiber results incorrectly classified as carbon fiber (Class 1) will be listed in the top right quadrant; the amount of carbon fiber results incorrectly classified as glass fiber will be listed in the bottom left quadrant; and the amount of carbon fiber results correctly classified will be listed in the bottom right quadrant.

(class 1). The FLD and SVM with a 'linear & polynomial' kernel made no classification mistakes as each had an F1 score of 1.00 (a perfect score). The optimized coefficients classification was not comparable with an F1 score of only 0.58. The classification was overfitting the carbon class (class 1) with over 60% of the glass data being incorrectly identified as carbon data. The overfitting behavior was an interesting outcome considering the optimization results indicated the glass-optimized coefficients gave a better fit to the data. For its low F1 score and poor classification results, Equation (5) was not considered capable of differentiating fiber type. The fact the AI-based Equation (5) resembled similar historical models yet vastly underperformed in the classification demonstrate the degree of information lost by the expressions in the Dispersion Region. This also showed that the dampening effects of the polymer and fibers had a greater effect on the attenuation within the Dispersion Region.

Attempting to determine to what extent the two fiber types could be correctly classified by the machine learning models, the recorded signals for the Dispersion region were divided into training and validation sets on a 2:1 ratio. The validation set was data the classifier had never seen before. The confusion matrices for the training and validation results for the four classifiers can be seen in Figure 6, demonstrating exceptional results. The FLD and SVM with a 'linear & polynomial' kernel were able to correctly classify the entirety of the training data, having a training F1 score of 1.00. All three classifiers were also able to correctly classify almost the entirety of the validation data as either a glass or carbon sample, having validation F1 scores of 1.00, 0.94, and 1.00, respectively. The SVM radial basis function kernel yielded lower training and validation F1 scores of 0.83 and 0.80, respectively, as it overfit the glass-based classifications.

The strong differentiation by the machine learning classification methods answers the above question of the capability in differentiating an unknown composite specimen based on their fiber type using their attenuation spectra. Fiber type seemed to be a differentiating factor for the attenuation spectra, even in regions where the fiber content and porosity had no significant effect. The smaller densities and higher moduli for the carbon fibers compared to glass fibers result in faster speeds of sound as the acoustic waves propagate through these materials, which were successfully captured using the machine learning models.

4 | Conclusions

The attenuation spectra of two heterogeneous composite materials were analyzed based on their dependency on porosity and fiber content, and mathematical expressions were conceived based on those findings to fit the data. Two distinct regions were identified having vastly different attenuation behaviors. Porosity and fiber content were determined to be significant influential factors on attenuation within the window of 250–310 kHz, with that influence successfully modeled using genetic programming. For example, a 1% increase in either porosity or fiber content increased attenuation by 4.86% (for the glass fibers) or 0.571%, respectively, in this region. Two expressions appeared to capture this and explained the effects of dispersion modes and fiber resonance on a propagating sound wave, though only one of these expressions properly accounted for all parameters appropriately. The influences of the dispersion modes and fiber resonance were much more prevalent for glass fiber-filled composites over carbon fiber-filled. Neither porosity nor fiber content affected the attenuation spectrum within the

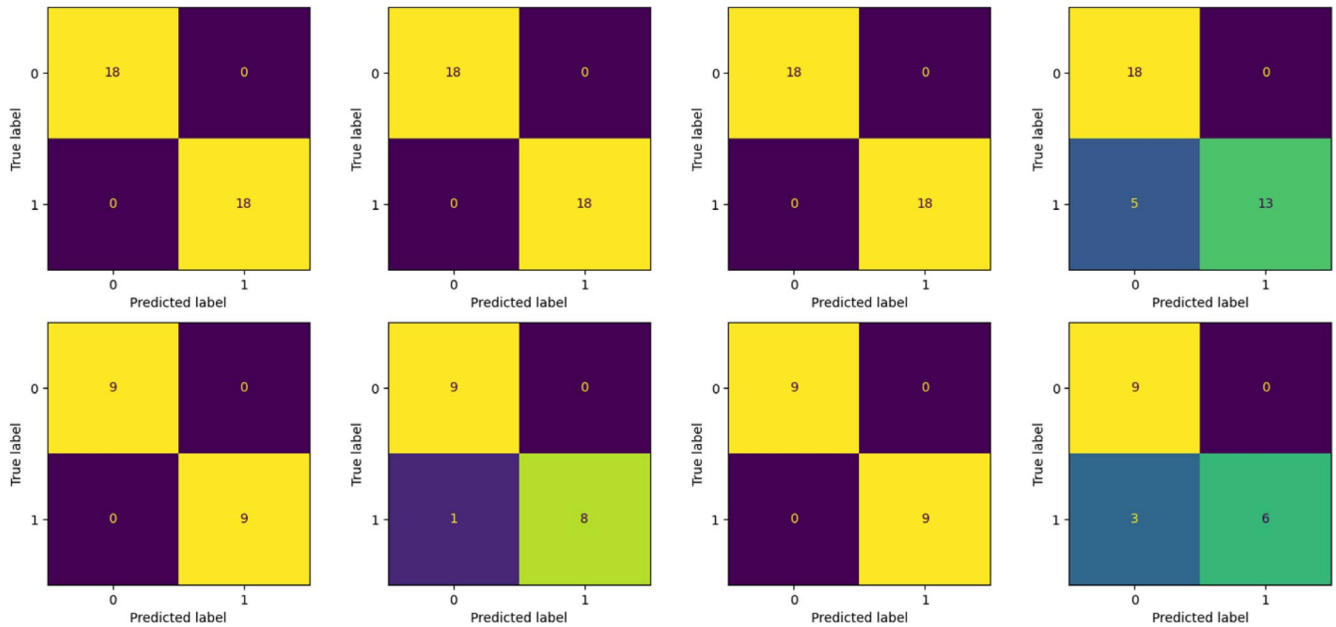

FIGURE 6 | Confusion matrix results for the four classification algorithms used when the data is split into 66% training and 33% validation. From left to right the confusion matrices are for Fisher's linear discriminant, support vector machine with a linear kernel, support vector machine with a polynomial kernel and a support vector machine with a radial basis function kernel. The top four confusion matrices are the training data results, and the bottom four confusion matrices are for the validation results. The amount of glass fiber results (Class 0) that were correctly classified will be listed in the top left quadrant, the amount of glass fiber results incorrectly classified as carbon fiber (Class 1) will be listed in the top right quadrant, the amount of carbon fiber results incorrectly classified as glass fiber will be listed in the bottom left quadrant, and the amount of carbon fiber results correctly classified will be listed in the bottom right quadrant.

second tested region defined by a window of 310–500 kHz, instead demonstrating sole reliance on the signal frequency, with respect to the fiber type, in very much a similar manner to homogeneous attenuation models. The attenuation spectra showed clear differentiation in our analyses based on fiber type, which was attributed to the material dampening coefficients having a primary role on signal loss.

It Is foreseeable by the mathematical expressions derived in this study that quality assurance based on acoustic monitoring could not only identify a fault in a prepared fiber-filled polymer composite but also point toward the most likely problematic factor.

Author Contributions

Austin D. Bedrosian: writing – original draft, investigation, methodology, validation. **Andrew Hrymak:** methodology, supervision, writing – review and editing. **Gisela Lanza:** resources, methodology, supervision. **Michael R. Thompson:** conceptualization, funding acquisition, writing – review and editing, supervision, resources.

Acknowledgments

The authors would like to thank both the NSERC Collaborative Research and Training Experience (CREATE) Program: Advanced Polymer Composite Materials and Technologies No. 401209347 and the Deutsche Forschungsgemeinschaft (DFG, German Research Foundation), project number 255730231, within the International Research Training Group "Integrated engineering of continuous-discontinuous long fiber-reinforced polymer structures" (GRK 2078) for the joint funding of this project. They also would like to thank Katja Höger, Jork Groenewold for aid during the μCT trials; the Karlsruhe Institute of Technology Institute of Production Science for hosting an international research exchange in Karlsruhe, Germany; and Dr. Ying Fan, Dr. Jeffrey Wood and Ariane van Elst for aid in the logistics of the international exchange.

Funding

This work was supported by the Natural Sciences and Engineering Research Council of Canada and Deutsche Forschungsgemeinschaft.

Conflicts of Interest

The authors declare no conflicts of interest.

Data Availability Statement

Data will be made available on request.

References

1. P. Osterrieder, L. Budde, and T. Friedli, "The Smart Factory as a Key Construct of Industry 4.0: A Systematic Literature Review," *International Journal of Production Economics* 221 (2020): 107476, https://doi.org/10.1016/j.ijpe.2019.08.011.

2. L. Zhang, C. Borigo, S. Owens, et al., "Ultrasonic Nonlinear Guided Wave Inspection of Microscopic Damage in a Composite Structure," *AIP Conference Proceedings* 1806 (2017): 020010, https://doi.org/10.1063/1.4974551.

3. C. J. Lissenden, Y. Liu, and J. L. Rose, "Use of Non-Linear Ultrasonic Guided Waves for Early Damage Detection," *Insight-Non-Destructive Testing and Condition Monitoring* 57 (2015): 206–211, https://doi.org/10.1784/insi.2015.57.4.206.

4. D. R. Françla, C. K. Jen, K. T. Nguyen, et al., "Ultrasonic In-Line Monitoring of Polymer Extrusion," *Polymer Engineering & Science* 40 (2004): 82–94, https://doi.org/10.1002/pen.11141.

5. R. Edwards and C. Thomas, "On-Line Measurement of Polymer Orientation Using Ultrasonic Technology," *Polymer Engineering and Science* 41 (2001): 1644–1653, https://doi.org/10.1002/pen.10862.

6. A. D. Bedrosian, M. R. Thompson, A. Hrymak, and G. Lanza, "Developing a Supervised Machine-Learning Model Capable of Distinguishing Fiber Orientation of Polymer Composite Samples Nondestructively Tested Using Active Ultrasonics," *Journal of Advanced Manufacturing and Processing* 5 (2022): e10138, https://doi.org/10.1002/amp2.10138.

7. C. C. Cheng, H. Banakar, B. T. Ooi, and C.-K. Jen, "Melting Quality of Polymers in Internal Mixer Diagnosed by Ultrasound," *International Polymer Processing* 24 (2009): 375–383, https://doi.org/10.3139/217.2166.

8. W. Punurai, J. Jarzynski, J. Qu, K. E. Kurtis, and L. J. Jacobs, "Characterization of Entrained Air Voids in Cement Paste With Scattered Ultrasound," *NDT & E International* 39 (2006): 514–524, https://doi.org/10.1016/j.ndteint.2006.02.001.

9. W. P. Mason and H. J. McSkimin, "Attenuation and Scattering of High Frequency Sound Waves in Metals and Glasses," *Journal of the Acoustical Society of America* 19 (1947): 464–473, https://doi.org/10.1121/1.1916504.

10. S. K. Datta, "A Self-Consistent Approach to Multiple Scattering by Elastic Ellipsoidal Inclusions," *Journal of Applied Mechanics* 44 (1977): 657–662, https://doi.org/10.1115/1.3424153.

11. S. Biwa, "Independent Scattering and Wave Attenuation in Viscoelastic Composites," *Mechanics of Materials* 33 (2001): 635–647, https://doi.org/10.1016/s0167-6636(01)00080-1.

12. A. D. Bedrosian, "Non-Destructive Quality Assurance of Fiber-Reinforced Polymer Composites Using Active Ultrasonics," Doctoral diss., McMaster University, 2025.

13. H. Jeong and D. K. Hsu, "Experimental Analysis of Porosity-Induced Ultrasonic Attenuation and Velocity Change in Carbon Composites," *Ultrasonics* 33 (1995): 195–203, https://doi.org/10.1016/0041-624x(95)00023-v.

14. A. El-Sabbagh, L. Steuernagel, and G. Ziegmann, "Characterisation of Flax Polypropylene Composites Using Ultrasonic Longitudinal Sound Wave Technique," *Composites, Part B: Engineering* 45 (2013): 1164–1172, https://doi.org/10.1016/j.compositesb.2012.06.010.

15. D. E. W. Stone and B. Clarke, "Ultrasonic Attenuation as a Measure of Void Content in Carbon-Fibre Reinforced Plastics," *Non-Destructive Testing* 8 (1975): 137–145, https://doi.org/10.1016/0029-1021(75)90023-7.

16. I. M. Daniel, S. C. Wooh, and I. Komsky, "Quantitative Porosity Characterization of Composite Materials by Means of Ultrasonic Attenuation Measurements," *Journal of Nondestructive Evaluation* 11 (1992): 1–8, https://doi.org/10.1007/bf00566012.

17. A. A. Karabutov, N. B. Podymova, and I. O. Belyaev, "The Influence of Porosity on Ultrasound Attenuation in Carbon Fiber Reinforced Plastic Composites Using the Laser-Ultrasound Spectroscopy," *Acoustical Physics* 59 (2013): 667–673, https://doi.org/10.1134/s1063771013060080.

18. J. Shi, W. Wang, F. Liu, G. Xun, and P. Yang, "Effects of Porosity on Ultrasonic Attenuation Coefficient, Shear Properties and Failure Mechanisms of CF/EP Laminates," *Heliyon* 10 (2024): e25288, https://doi.org/10.1016/j.heliyon.2024.e25288.

19. Z. Han, S. Jeong, J.-W. Jang, J. H. Woo, and D. Oh, "Ultrasonic Attenuation Characteristics of Glass-Fiber-Reinforced Polymer Hull Structure," *Applied Sciences* 11 (2021): 6614, https://doi.org/10.3390/app11146614.

20. A. D. Bedrosian, A. Hrymak, G. Lanza, and M. R. Thompson, "Understanding a Frequency Shifting Phenomenon Interfering With

In-Line Acoustic Monitoring of an Extrusion Compounding Process for Polymer Composites," *Journal of Thermoplastic Composite Materials* 38 (2025): 08927057251321492, https://doi.org/10.1177/08927057251321492.

21. Physical Acoustics, "R30a—300 kHz General Purpose AE Sensor," https://www.physicalacoustics.com/by-product/sensors/R30a-300-kHz-General-Purpose-AE-Sensor.

22. C. R. Harris, K. J. Millman, S. J. van der Walt, et al., "Array Programming With NumPy," *Nature* 585 (2020): 357–362, https://doi.org/10.1038/s41586-020-2649-2.

23. F. Rotea, "Lamb-Wave-Dispersion," https://github.com/franciscorotea/Lamb-Wave-Dispersion.

24. "Datasheet for E-Glass Fiber, Generic," https://www.matweb.com/search/datasheet.aspx?MatGUID=d9c18047c49147a2a7c0b0bb1743e812.

25. M. Minus and S. Kumar, "The Processing, Properties, and Structure of Carbon Fibers," *JOM* 57 (2005): 52–58, https://doi.org/10.1007/s11837-005-0217-8.

26. L. C. Pardini and L. G. B. Manhani, "Influence of the Testing Gage Length on the Strength, Young's Modulus and Weibull Modulus of Carbon Fibres and Glass Fibres," *Materials Research* 5 (2002): 411–420, https://doi.org/10.1590/S1516-14392002000400004.

27. Designer Data, "Thermoplastics—Polypropylene," https://designerdata.nl/materials/plastics/thermo-plastics/polypropylene-(cop.).

28. F. P. C. Gomes and M. R. Thompson, "Analysis of Mullins Effect in Polyethylene Using Ultrasonic Guided Waves," *Polymer Testing* 60 (2017): 351–356, https://doi.org/10.1016/j.polymertesting.2017.04.020.

29. T. L. Szabo, "Causal Theories and Data for Acoustic Attenuation Obeying a Frequency Power Law," *Journal of the Acoustical Society of America* 97 (1995): 14–24, https://doi.org/10.1121/1.412332.

30. Z. Guezzen, L. Errouane, Z. Hammou, A. Boussoufi, and Z. Sereir, "Effect of Fiber Content and Curvature on Probabilistic Free Vibration Analysis of Cylindrical Shallow Shells Reinforced by Short Natural Fibers," *Industrial Crops and Products* 197 (2023): 116480, https://doi.org/10.1016/j.indcrop.2023.116480.

31. E. Youn, L. Koenig, M. K. Jeong, and S. H. Baek, "Support Vector-Based Feature Selection Using Fisher's Linear Discriminant and Support Vector Machine," *Expert Systems with Applications* 37 (2010): 6148–6156, https://doi.org/10.1016/j.eswa.2010.02.113.

Supporting Information

Additional supporting information can be found online in the Supporting Information section. **Figure S1:** Average calculated attenuation coefficients (Np/mm) for both glass fiber (blue) and carbon fiber (black) reinforced polypropylene composites in the region of symmetry with a testing range of 250 to 310 kHz. The frequency resolution is every 1 kHz. The solid lines (–) represent the 5 vol% results, the dashed lines (– – –) represent the 15 vol% results and the dotted lines (· · ·) represent the 25 vol% data. **Figure S2:** Micro-computed tomography scan diameter distributions for both (A) a glass fiber reinforced plaque and (B) a carbon fiber reinforced plaque. **Figure S3:** Average calculated attenuation coefficients (Np/mm) plotted with the standard deviation at each respective frequency (kHz) for both (A) the glass fiber results and (B) the carbon fiber results. The **green** lines are the 5 vol% results, the **orange** lines are the 15 vol% results, and the **black** lines are the 25 vol% results.